### Title

Aeroacoustics of volcanic jets: Acoustic power estimation and jet velocity dependence




### Journal

J. Geophys. Res. Solid Earth, 118



### Authors

Matoza, Robin S

Fee, D

Neilsen, Tracianne B

et al.



### Publication Date

2013-12-26

Peer reviewed

JOURNAL OF GEOPHYSICAL RESEARCH: SOLID EARTH, VOL. 118, 1–16, doi:10.1002/2013JB010303, 2013

# Aeroacoustics of volcanic jets: Acoustic power estimation and jet velocity dependence

Robin S. Matoza,[1] David Fee,[2] Tracianne B. Neilsen,[3] Kent L. Gee,[3] and Darcy E. Ogden[1]

Received 18 April 2013; revised 18 November 2013; accepted 21 November 2013.

[1] A fundamental goal of volcano acoustics is to relate observed infrasonic signals to the eruptive processes generating them. A link between acoustic power $\overline{\Pi}$ and volcanic gas exit velocity $V$ was proposed by Woulff and McGetchin (1976) based upon the prevailing jet noise theory at the time (acoustic analogy theory). We reexamine this approach in the context of the current understanding of jet noise, using data from a laboratory jet, a full-scale military jet aircraft, and a full-scale rocket motor. Accurate estimates of $\overline{\Pi}$ require good spatial sampling of jet noise directionality; this is not usually possible in volcano acoustic field experiments. Typical volcano acoustic data better represent point measurements of acoustic intensity $\bar{I}(\theta)$ at a particular angle $\theta$ from the jet axis rather than $\overline{\Pi}$. For pure air jet flows, velocity-scaling laws currently proposed for acoustic intensity differ from those for acoustic power and are of the form $\bar{I}(\theta) \sim (V/c)^{n_\theta}$, where $c$ is the ambient sound speed and $n_\theta$ varies nonlinearly from ~5 to 10 as a function of temperature ratio and angle $\theta$. Volcanic jet flows are more complex than the pure air laboratory case, which suggests that we do not currently know how the exponent $n_\theta$ varies for a volcanic jet flow. This indicates that the formulation of Woulff and McGetchin (1976) can lead to large errors when inferring eruption parameters from acoustic data and thus requires modification. Quantitative integration of field, numerical, and laboratory studies within a modern aeroacoustics framework will lead to a more accurate relationship between volcanic infrasound and eruption parameters.

**Citation:** Matoza, R. S., D. Fee, T. B. Neilsen, K. L. Gee, and D. E. Ogden (2013), Aeroacoustics of volcanic jets: Acoustic power estimation and jet velocity dependence, *J. Geophys. Res. Solid Earth*, *118*, doi:10.1002/2013JB010303.

## 1. Introduction

[2] Jet flow, the sustained and momentum-driven flux of fluid from a nozzle or vent, occurs in both natural (e.g., volcanoes and geysers) and man-made settings (e.g., the exhaust from jet engines and rockets) [*Kundu and Cohen*, 2008; *Kieffer and Sturtevant*, 1984]. It is now well known that a broad range of volcanic eruption styles produce a diverse range of acoustic signals <20 Hz, termed *infrasound* [e.g., *Johnson and Ripepe*, 2011; *Fee and Matoza*, 2013; *Garces et al.*, 2013]. This paper focuses on the infrasound produced by volcanic jet flows [*Matoza et al.*, 2009a; *Fee et al.*, 2010a, 2010b]. Constraining parameters of volcanic jet flows is important for understanding explosive volcanic eruptions and for mitigating their hazards [*Sparks et al.*, 1997]. In order to infer volcanic jet parameters (e.g., jet velocity or diameter) from infrasound data, a quantitative link between the volcanic jet flow and its radiated infrasound is required. Such a quantitative link could ultimately be used to place constraints on, e.g., plume height, column stability, and ash release based on infrasound data [*Vergniolle and Caplan-Auerbach*, 2006; *Garces et al.*, 2008; *Matoza et al.*, 2009a; *Fee et al.*, 2010a; *Caplan-Auerbach et al.*, 2010; *Dabrowa et al.*, 2011; *Ripepe et al.*, 2013].

[3] Recent work has suggested that eruptions involving volcanic jet flows generate a low-frequency (infrasonic) form of the aeroacoustic jet noise produced by smaller scale man-made jets [*Matoza et al.*, 2009a; *Fee et al.*, 2010a, 2010b, 2013]. Jet noise is the noise generated by a turbulent jet flow itself. Man-made jet noise has been extensively studied for noise and vibration control purposes [e.g., *Tam*, 1998]. In the case of aircraft or rockets, "jet noise" refers only to the sound generated by the turbulent exhaust (a jet flow) issuing out of the jet engine or rocket. Other sources of noise from flight vehicles resulting from, e.g., their motion through the air, rotor noise, or turbomachinery noise are not classed as "jet noise". These other sources have different characteristics and are of course not expected from a volcano [see *Hubbard*, 1991 for a comprehensive review]. Aeroacoustics is the study of

[1]Institute of Geophysics and Planetary Physics, Scripps Institution of Oceanography, La Jolla, California, USA.
[2]Wilson Infrasound Observatories, Alaska Volcano Observatory, Geophysical Institute, University of Alaska Fairbanks, Fairbanks, Alaska, USA.
[3]Department of Physics and Astronomy, Brigham Young University, Provo, Utah, USA.

Corresponding author: R. S. Matoza, Institute of Geophysics and Planetary Physics, Scripps Institution of Oceanography, La Jolla, CA 92093-0225, USA. (rmatoza@ucsd.edu)


2169-9313/13/10.1002/2013JB010303

sound generated as a byproduct of a fluid flow, including jet noise.

[4] This paper explores, within the context of the present day understanding of jet noise, the practice of estimating acoustic power levels and jet velocities from acoustic pressure measurements. Previous studies in the field of volcano acoustics have used results from the classical aeroacoustics literature to link acoustic signals with volcanic gas exit velocity [e.g., *Woulff and McGetchin*, 1976; *Vergniolle and Caplan-Auerbach*, 2006; *Caplan-Auerbach et al.*, 2010; *Ripepe et al.*, 2013]. However, some of the key results used in these studies have largely been abandoned in modern aeroacoustics research [e.g., *Tam et al.*, 2008; *Viswanathan*, 2009]. In this paper, we highlight results from modern jet noise research and discuss their implications for volcano acoustics.

[5] The pioneering study by *Woulff and McGetchin* [1976] introduced the idea of using radiated acoustic power and frequency content to infer gas exit velocity for eruptions involving vigorous release of volcanic gases. This represents a first attempt at a quantitative framework relating volcanic fluid mechanics and acoustic wave generation. *Woulff and McGetchin* [1976] measured sound-pressure level (SPL) (see Appendix A) near volcanic fumaroles. They then used SPL to estimate the overall sound power level (OAPWL) (see Appendix A) by assuming an acoustic source radiating sound equally in all directions (i.e., no source directionality and spherically symmetric source). Finally, they used results from the classical aeroacoustics literature [*Lighthill*, 1962, 1963; *Curle*, 1955] to relate the total acoustic power $\overline{\Pi}$ (related to OAPWL, see Appendix A) with the gas exit velocity $V$

$$\text{Monopole} \quad \overline{\Pi}_M = K_M \frac{\rho_0 A_v}{c} V^4, \tag{1}$$

$$\text{Dipole} \quad \overline{\Pi}_D = K_D \frac{\rho_0 A_v}{c^3} V^6, \tag{2}$$

$$\text{Quadrupole} \quad \overline{\Pi}_Q = K_Q \frac{\rho_0 A_v}{c^5} V^8, \tag{3}$$

where $\overline{\Pi}_M$, $\overline{\Pi}_D$, and $\overline{\Pi}_Q$ are the acoustic power radiated by equivalent monopole, dipole, and quadrupole sources, respectively, (see section 2); $A_v$ is the volcanic vent area; $\rho_0$ is the ambient density; and $c$ is the ambient sound speed. The coefficients of proportionality in each case $K_M$, $K_D$, and $K_Q$ were termed the "acoustic power coefficient" in the original work by *Lighthill* [1952, 1954].

[6] Although *Woulff and McGetchin* [1976] only considered acoustic signals >20 Hz, recent infrasound studies have built extensively upon their formulation [e.g., *Vergniolle and Caplan-Auerbach*, 2006; *Caplan-Auerbach et al.*, 2010; *Ripepe et al.*, 2013] (note that theory developed for audible acoustic frequencies is generally valid for infrasound down to the acoustic cutoff frequency, which is about 3.3 mHz in the lower atmosphere; [*Evers and Haak*, 2010]). Extensions to the study by *Woulff and McGetchin* [1976] have included solving equations (2)–(3) for $V$ and then using $V$ to infer plume height or mass eruption rate, which are then compared with other data used to constrain these paramaters [e.g., *Vergniolle and Caplan-Auerbach*, 2006; *Caplan-Auerbach et al.*, 2010; *Delle Donne and Ripepe*, 2012; *Ripepe et al.*, 2013].

[7] The structure of this paper is as follows. We begin in section 2 by providing a brief background in equivalent sources, jet noise, and the origin of equations (2)–(3). In section 3, we reexamine the process of converting SPL measurements to acoustic power $\overline{\Pi}$ in light of present-day understanding of jet noise directionality, i.e., knowledge of how SPL measurements vary with angle from the jet axis. We use laboratory jet, full-scale military jet aircraft, and full-scale rocket motor noise data to illustrate directionality effects. In section 4, we reexamine the critical relations between acoustic power and jet velocity (equations (2)–(3)) in light of modern aeroacoustics research. In particular, we show that equations (2)–(3) have largely been abandoned and replaced in the aeroacoustics literature based upon detailed laboratory studies of jet noise. In sections 2–4, we use results from man-made jet flows to illustrate the basic issues in attempts to quantify the infrasound radiated by large-scale volcanic jet flows. Deviations of volcanic jet flows from the case of man-made jets are then discussed in section 5.

## 2. Background

### 2.1. Equivalent Sources

[8] We begin with a brief review of equivalent sources in linear acoustic theory (for more details, see, e.g., *Morse and Ingard* [1968], *Lighthill* [1962, 1978], and *Pierce* [1989]). Acoustic source processes may be very complex; however, outside a theoretical surface bounding any arbitrary source, the source can be represented as a sum of equivalent sources provided that the source region is *compact*, i.e., small compared to $\lambda/2\pi$, where $\lambda$ is the wavelength (for reference, $c = f\lambda$ gives $\lambda \sim 330$ m for 1 Hz infrasound). The most elementary source is one that radiates sound equally in all directions; this is called a "simple source", "point source", or "monopole" (Figure 1a). The acoustic pressure at a time $t$ and distance $r$ from a monopole source is given by [*Lighthill*, 1978]

$$p(t,r) = \frac{\dot{q}(t - r/c)}{4\pi r}, \tag{4}$$

where $\dot{q}(t)$ is the *rate of change* of the rate of mass outflow (also called the *source strength*) and $c$ is the sound speed. A consequence of equation (4) is that steady gas exit velocity does not generate sound; only fluctuations from a mean gas exit velocity generate sound [*Lighthill*, 1978]. The first few seconds of an impulsive volcanic explosion (blast-type eruption), which involves a rapid acceleration of the atmosphere, can often be well approximated by a monopole [*Woulff and McGetchin*, 1976; *Johnson*, 2003; *Fee and Matoza*, 2013].

[9] The next elementary source is the acoustic dipole, which is formed by two monopoles of equal strength, but oscillating in opposite phase, $\dot{q}(t)$ and $-\dot{q}(t)$, separated by a small distance (Figure 1b). Whereas the monopole is associated with time-varying mass flux (equation (4)), the dipole is equivalent to force or momentum changes acting on the fluid. The dipole is a directional source, with the dipole strength being a vector with magnitude equal to the force [*Lighthill*, 1962, 1978]. Just as two monopoles can be combined to form a dipole, two dipoles can be combined to form a quadrupole (Figures 1c and 1d).

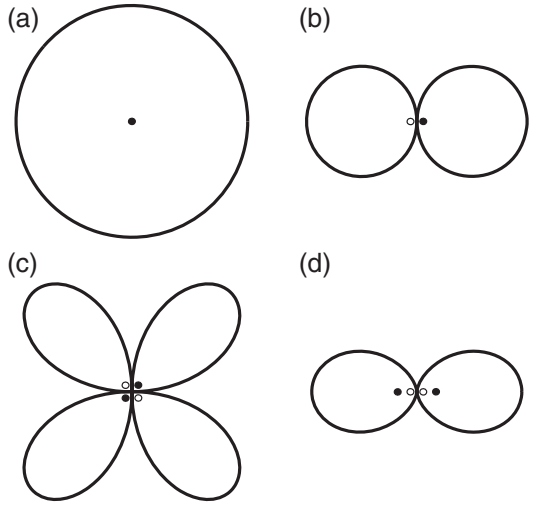


**Figure 1.** Radiation patterns of the acoustic (a) monopole, (b) dipole, (c) lateral quadrupole, and (d) longitudinal quadrupole. The distance from the origin to the point on the surface is proportional to the absolute value of acoustic pressure in that direction. The black and white dots represent monopoles with positive and negative signs at this time snapshot, respectively. See *Pierce* [1989] for more details. Even though an individual theoretical quadrupole is highly directional (Figures 1c and 1d), a random arrangement of quadrupoles as proposed by *Lighthill* [1962] can radiate isotropically.

### 2.2. Acoustic Analogy Theory

[10] The pioneering studies of *Lighthill* [1952, 1954] marked the beginning not only of jet noise research, but also of the field of aeroacoustics [*Tam*, 1998]. *Lighthill* [1952, 1954, 1963] developed the acoustic analogy theory, in which he manipulated the compressible equations of motion into the form of an inhomogeneous wave equation

$$\frac{\partial^2 \rho}{\partial t^2} - c^2 \nabla^2 \rho = \frac{\partial^2 T_{ij}}{\partial x_i \partial x_j}, \tag{5}$$

where $\rho$ is the density (small acoustic perturbations from ambient), $c$ is the ambient sound speed, and

$$T_{ij} = \rho u_i u_j + (p - \rho c^2)\delta_{ij} - \tau_{ij} \tag{6}$$

is the Lighthill stress tensor, with $u_i$ the acoustic particle velocity, $p$ the acoustic pressure, $\tau_{ij}$ the viscous (shear) stresses, and $\delta_{ij}$ the Kronecker delta; the summation convention is assumed.

[11] The left-hand side of equation (5) describes wave propagation, while the right-hand side denotes the inferred source terms. The source terms involve second spatial derivatives; the first term $\rho u_i u_j$ in equation (6) is termed the quadrupole. Lighthill proposed that jet noise consists of a distribution of randomly oriented quadrupoles, with an equivalent quadrupole strength $T_{ij} \approx \rho u_i u_j$ per unit volume [*Lighthill*, 1962, 1963]. The prevailing view in the 1950s was that these quadrupoles were somehow related to small turbulent eddies in the jet flow, although no formal relationship was ever established [*Tam*, 1998]. We note that even though an individual theoretical quadrupole is highly directional (Figures 1c and 1d), a random arrangement of quadrupoles can radiate isotropically. Note that jet noise directionality, described in sections 3 and 4, is different.

[12] The acoustic analogy theory was extended by *Curle* [1955] to consider aeroacoustic source processes influenced by a solid boundary. *Curle* [1955] proposed that such a source is equivalent to a distribution of dipoles, corresponding to the force per unit area acting on the flow by the boundary. As introduced in section 1, results from these early studies using acoustic analogy theory [*Lighthill*, 1952, 1954; *Curle*, 1955] were applied to volcanoes by *Woulff and McGetchin* [1976]. *Woulff and McGetchin* [1976] considered blast-type eruptions [i.e., explosions; see *Johnson*, 2003; *Fee and Matoza*, 2013] to be mostly monopole in nature. They further considered jet noise as composed of quadrupoles, or dipoles if solid boundaries are present, e.g., if solid particles are entrained or if a jet flow interacts with solid vent walls. As we can see, this was the prevailing view of jet noise at the time [*Lighthill*, 1954, 1963; *Curle*, 1955].

[13] However, many modifications and extensions to acoustic analogy theory were subsequently proposed [see reviews by *Lilley*, 1991; *Tam*, 1998; *Tam et al.*, 2008; *Viswanathan*, 2009, and references therein], none of which have been considered in the volcano acoustics literature. Important modifications included attempts to include moving sources, temperature effects, and the highly directional nature of jet noise as revealed by laboratory experiments, which could not be explained by the more basic formulations of *Lighthill* [1952] and *Curle* [1955]. For example, some extensions of acoustic analogy theory argued that jet noise consists of not just dipoles and quadrupoles, but monopoles as well [*Viswanathan*, 2009, and references therein]. However, in the 1970s, coherent structures were identified in turbulence [e.g., *Crow and Champagne*, 1971]. Soon afterward, coherent turbulence structures were recognized as important jet noise sources [*Tam*, 1998]. From the 1970s and 1980s onward, jet noise studies underwent a fundamental shift away from acoustic analogy theory [*Tam*, 1998] (see section 2.3).

### 2.3. Modern Jet Noise Studies

[14] In current jet noise studies, the idea of jet noise as composed of equivalent sources of monopoles, dipoles, and quadrupoles has largely been abandoned [*Tam*, 1998; *Tam et al.*, 2008; *Viswanathan*, 2009]. Jet noise is characterized in laboratory and field aeroacoustics studies by considering how acoustic signal properties vary as a function of angle to the jet axis (angle $\theta$; Figure 2a) and jet operating parameters such as the jet velocity, diameter, temperature, density, and nozzle geometry. These data indicate that there are three main components of jet noise: (1) jet mixing noise, (2) broadband shock-associated noise, and (3) screech tones. For simplicity, we only consider the jet mixing noise component (1) in this paper. Jet mixing noise (1) is the most basic component of jet noise and appears to be relevant for volcanic jets [*Matoza et al.*, 2009a]. Broadband shock-associated noise (2) and screech tones (3) both require well-formed and steady internal shock structures, which are difficult to achieve in volcanic systems because of, e.g., nozzle irregularity, lithics, or tephra larger than fine ash, wind, and evolution of vent shape. In addition, jet noise research indicates that strong broadband shock-associated noise is not

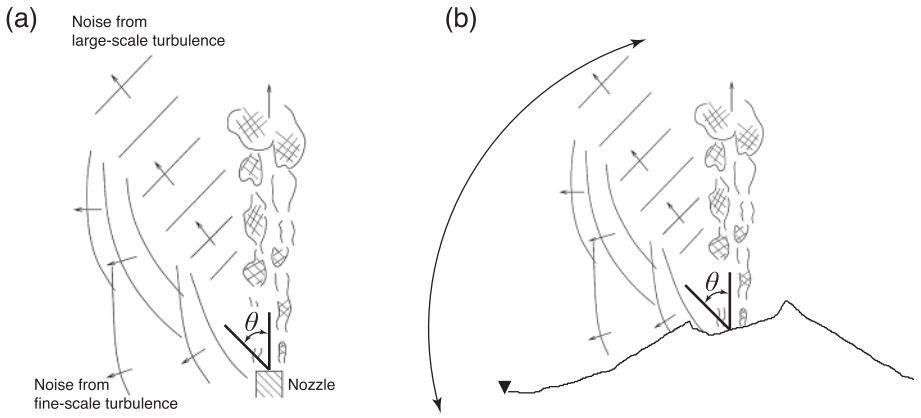


**Figure 2.** (a) Cartoon illustrating the dominant radiation directions of the two sources of jet mixing noise as a function of angle from the jet axis $\theta$, as determined from laboratory experiments [*Tam et al.*, 1996; *Tam*, 1998; *Tam et al.*, 2008]. The two jet mixing noise sources are the fine-scale turbulence (FST) and large-scale turbulence (LST). Laboratory jet noise characteristics are highly directional, i.e., a strong function of angle from the jet axis $\theta$. (b) In the case of volcano acoustics field experiments, sampling of the hypothesized volcanic jet noise as a function of angle from the jet axis (arc with arrowheads) is not usually possible; we are typically restricted to observations at a limited angular range, e.g., the infrasound sensor indicated as a black triangle (see also Figure 3). The figure is modified from *Tam et al.* [2008].

seen for military jet or rocket noise [*Neilsen et al.*, 2013a]. Laboratory-scale measurements suggest that the broadband shock-associated noise saturates while the mixing noise continues to increase with temperature [*Viswanathan et al.*, 2010].

[15] We also do not consider noise generation processes involving the interaction of a jet flow with solid boundaries such as vent walls, considering only the case of a free jet. While volcanic jets probably interact with the shallow conduit structure and vent walls (see section 5), this additional complication is beyond the scope of the present study.

[16] For jet mixing noise (1), laboratory data support a two-source model, composed of the noise from (a) fine-scale turbulence (FST), and (b) large-scale turbulence (LST) [*Tam et al.*, 1996]. The primary difference between modern jet noise studies and studies based on the acoustic analogy is the recognition of the importance of coherent structures within the jet flow. In the acoustic analogy framework, sound results from small-scale and incoherent turbulent eddies. In contrast, LST noise is modeled by the growth and decay of stochastic instability waves (coherent structures) propagating downstream at the edge of the jet flow in the shear layer between the jet flow and ambient atmosphere (Figure 2a) [*Tam and Burton*, 1984].

[17] We point out for clarity that LST noise, which was proposed as a source mechanism by *Matoza et al.* [2009a], is not quadrupole radiation. This is incorrectly cited in several recent papers [e.g., *Caplan-Auerbach et al.*, 2010; *Kim et al.*, 2012; *Delle Donne and Ripepe*, 2012; *Ripepe et al.*, 2013; *Johnson et al.*, 2013].

### 2.4. Acoustic Power vs. Gas Exit Velocity in Acoustic Analogy Theory

[18] In the original acoustic analogy formulation, *Lighthill* [1962, 1963] performed dimensional analysis. The dimensional analysis predicts that the total acoustic power ($\overline{\Pi}$ or OAPWL; see Appendix A) radiated by a jet varies with the eighth power of jet velocity; this is known as the $V^8$ law. More specifically, the total acoustic power is predicted to have a linear relationship with the Lighthill parameter

$$\frac{\rho_0 d^2 V^8}{c^5}, \tag{7}$$

where $\rho_0$ is the ambient air density, $d$ is a characteristic dimension of the flow, $V$ is the jet velocity, and $c$ is the ambient sound speed. A similar analysis by *Curle* [1955] predicted that the total acoustic power radiated by a flow past a solid boundary varies like $V^6$. These results were used by *Woulff and McGetchin* [1976] (equations (2)–(3)). Equations (2)–(3) can be written more generally

$$\overline{\Pi} = K\rho_0 A_v c^3 \left(\frac{V_j}{c}\right)^n, \tag{8}$$

where $n$ is 4, 6, or 8 and $K$ is an unknown acoustic power coefficient (see section 4.2).

[19] In sections 3 and 4, we reconsider these relationships (equation (8)) in light of modern aeroacoustics research. We address two fundamental and related issues. The first issue, which we address in section 3, concerns how the acoustic power $\overline{\Pi}$ (the quantity appearing on the left-hand side of equation (8)) is estimated. *Woulff and McGetchin* [1976] estimated $\overline{\Pi}$ by assuming isotropic radiation. They used a spherical spreading correction of $4\pi r^2$ to obtain $\overline{\Pi}$ from a point microphone measurement (i.e., they used equation (A4) in Appendix A). More recent infrasound studies have used a hemispherical correction of $2\pi r^2$ [*Garces et al.*, 2013]. In section 3 and Appendix A, we show that both of these assumptions (hemispherical or spherical correction) lead to incorrect results if the underlying source is not isotropic but actually directional. Jet noise is known to be highly directional (Figure 2a); thus assuming isotropic radiation in order to estimate $\overline{\Pi}$ will lead to erroneous results.

[20] The second issue, which we address in section 4, is that the relations between acoustic power and jet velocity shown in equation (8) have been revised and replaced

in current jet noise studies based upon detailed laboratory data. Additionally, volcano acoustics experiments represent point measurements of acoustic intensity rather than acoustic power and the relationships between acoustic intensity and jet velocity are different from those between acoustic power and jet velocity.

## 3. Jet Noise Directionality and Acoustic Power

[21] Jet noise is highly directional, i.e., jets do not radiate sound equally in all directions (Figure 2a). In this section, we show that reliable estimates of acoustic power $\overline{\Pi}$ are very difficult to obtain for volcanic jets because typical volcano-acoustics field experiments do not adequately sample the directionality of volcanic jet noise. It has been known that jet noise is directional since the first experimental jet noise studies [e.g., *Fitzpatrick and Lee*, 1952], even though this was not accounted for in the early acoustic analogy formulations [*Lighthill*, 1952, 1954; *Curle*, 1955; *Woulff and McGetchin*, 1976]. Thus, jet noise is not a simple source. The assumption of a spherical spreading correction of $4\pi r^2$ [*Woulff and McGetchin*, 1976], or a hemispherical correction of $2\pi r^2$, is therefore not valid if the acoustic source is a jet flow.

[22] For a directional source such as jet noise, estimating the acoustic power $\overline{\Pi}$ requires integration of measurements across a swath of angles covering the far-field directionality (Figure 2) (the far-field is defined as distances $r \gg \lambda/2\pi$). In the typical volcano acoustics field experiment, which is usually limited to observations on the ground surface with limited angular coverage of the volcanic jet (Figure 2b), sampling the jet noise directionality is not possible. In this section, we highlight the issues that may be encountered when trying to infer the total acoustic power $\overline{\Pi}$ radiated by a jet when the only data available are microphones at a limited angular range (Figure 2b). We do this using jet noise data recorded from jet flows with a variety of length-scales: a laboratory-scale jet, a full-scale military jet aircraft, and a full-scale reusable solid rocket motor. These systems represent different regimes of man-made jets with different radiation patterns, which we use to illustrate how $\overline{\Pi}$ estimates might vary.

[23] The jet noise directionality discussed in this section and shown in Figure 2 is different from (and not related to) the directionality of a single theoretical dipole or quadrupole as shown in Figure 1. The directionality of jet noise revealed in laboratory experiments is generally explained in terms of the angular regions of dominance of FST and LST noise sources (Figure 2a) [*Tam et al.*, 2008]. For pure-air laboratory jets, LST noise is usually dominant in a narrow angular region from the jet axis ($\theta$ less than $\sim 55°$), while FST noise is dominant at other angles [*Tam et al.*, 2008]. In general, the crossover point between LST and FST dominance occurs at different $\theta$ for different types of jet flows and jet conditions [*Neilsen et al.*, 2013a, 2013b], and there is an intermediate region where a mix of FST and LST noise components is observed [*Tam et al.*, 1996].

### 3.1. Acoustic Power Estimation

[24] In this section, we describe the estimation of acoustic power for isotropic and directional sound sources. In Appendix A, we clarify the difference between the acoustic intensity at a particular observation point from a source, and the acoustic power of the source. The acoustic power represents the total power radiated by the source, integrated over all angles, whereas the acoustic intensity represents the power per unit area at a particular observation angle. The acoustic power $\overline{\Pi}$ is the time-averaged rate of total acoustic energy flow radiated by the source with units of *watts* (W) (Appendix A). It is evaluated

$$\overline{\Pi} = \int_S \bar{\mathbf{I}} \cdot \mathbf{n}_{\text{out}} \, \mathrm{d}S, \tag{9}$$

where $\bar{\mathbf{I}}$ is the time-averaged acoustic intensity vector on a surface $S$ enclosing the source, and $\mathbf{n}_{\text{out}}$ is the outward pointing unit normal vector on that surface. This is often expressed logarithmically as the overall sound power level (OAPWL)

$$\text{OAPWL} = 10 \log_{10} \left( \frac{\overline{\Pi}}{\Pi_{\text{ref}}} \right), \tag{10}$$

where $\Pi_{\text{ref}}$ is the reference power of $10^{-12}$ W or 1 pW.

[25] For spherically symmetric waves (radiating equally in all directions), $\bar{\mathbf{I}}$ is in the radial direction and there is no variation in its magnitude with angle, and at a distance $r$ from the source in the far-field (and assuming no reflecting boundaries, i.e., the free-field case) the power can be recovered from

$$\overline{\Pi}_{\text{sph}} = 4\pi r^2 \bar{I}, \tag{11}$$

where $\bar{I}$ is the time-averaged radial component of intensity. For a directional source such as jet noise, however, equation (11) is not valid. Instead, the integral in equation (9) must be approximated. In practice, measurements are not made continuously over a surface; the power is estimated from a discrete set of measurements.

[26] In experiments designed to investigate jet noise directionality, measurements are taken along an arc in the far field (Figure 3). Typically, the mean-square pressure $\overline{p^2}$ is measured at a finite number of angles from the jet axis ($0° \leq \theta \leq 180°$, see Figures 2 and 3) in a single horizontal plane (defined as $\phi = 0$). To estimate power, an axisymmetric assumption is made to extend the measurements to multiple polar angles $\phi$ and approximate the normal component of the intensity over the surface of the sphere. Discrete surface area elements $\Delta S_{j,l}$ are defined to account for the surface area associated with each measured and extrapolated value. The power is then estimated by a double summation

$$\overline{\Pi} = \sum_{l=1}^{L} \sum_{j=1}^{J} \bar{I}_{j,l} \Delta S_{j,l}, \tag{12}$$

where $L$ is the number of sampled angles from the jet axis $\theta_l$, and $J$ is the number of polar angles $\phi$. For the axisymmetric case, the double sum collapses such that

$$\overline{\Pi} = \sum_{l=1}^{L} \overline{\Pi}_l = \sum_{l=1}^{L} \bar{I}(\theta_l) \Delta S(\theta_l). \tag{13}$$

The factor $\Delta S(\theta_l)$ is an area weighting factor, representing the effective sampling area per microphone on the measurement of a sphere of radius $r$ [*Leishman et al.*, 2006]. A more detailed explanation of $\Delta S$ is found in the work by

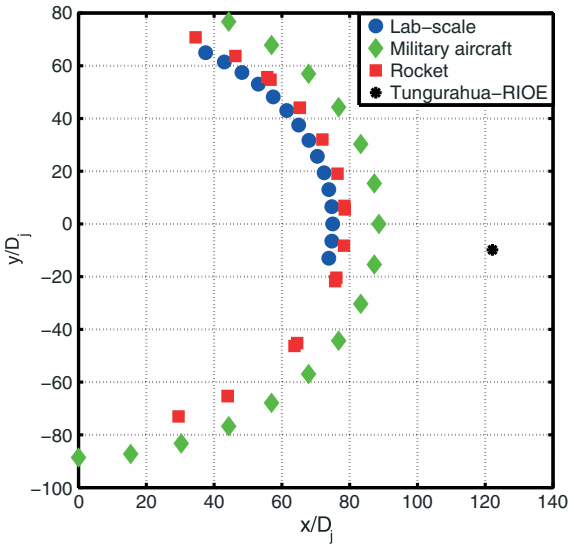


**Figure 3.** Measurement locations of jet noise directionality from a laboratory-scale jet, a full-scale military jet aircraft, and a full-scale rocket motor, as compared to a volcano acoustics field experiment at Tungurahua volcano. The measurement locations are scaled by the expanded jet diameter $D_j$. In the case of Tungurahua, $D_j$ is assumed to be 300 m. The nozzle exit is at approximately (0,0) and the exhaust is pointed in the positive direction along the $y$ axis.

*Leishman et al.* [2006], but the expressions for the axisymmetric case are

$$\Delta S(\theta_l) = \begin{cases} 4\pi r^2 \sin^2\left(\frac{\Delta\theta_l}{4}\right); & \text{for } l = 1, L \\ 4\pi r^2 \sin(\theta_l)\sin\left(\frac{\Delta\theta_l}{2}\right); & \text{for } 2 \le l \le L-1. \end{cases} \quad (14)$$

[27] We note that in this section, all of our acoustic power estimates are made for steady-state jet velocity conditions. Thus, because there is no variation in jet velocity, we do not consider the variations of acoustic power or intensity as a function of jet velocity that are considered later in section 4. Our aim is to show how acoustic power estimates require a decent sampling of jet noise directionality, which is a separate issue to the velocity dependence discussed in section 4.

### 3.2. Laboratory-Scale Jet

[28] We now present an example of how the method described in section 3.1 is employed to find the acoustic power of a laboratory-scale jet. We use data collected from a Mach 2.0, unheated jet with a 3.49 cm diameter nozzle [*Gee et al.*, 2010]. The jet flow geometry was horizontal and the data were recorded in an anechoic chamber. The data were recorded on Bruel and Kjaer 6.35 mm and 3.18 mm pressure microphones mounted at 75 nozzle diameters ($D_j$) on a boom that swept out a measurement arc between 30–100° (relative to the jet axis and to a reference position $4D_j$ downstream) in 5° increments (Figure 3). Note that it is conventional in jet noise studies to scale distances by the jet diameter $D_j$. The sampling rate was 192 kHz. The experimental setup is described in more detail by *Gee et al.* [2010].

[29] Figure 4a shows the acoustic intensity for each angle at a far-field distance of $75D_j$. Although good angular sampling was achieved in the experiment, we use a linear fit to extrapolate to angles greater than 100°, and a quadratic fit to extrapolate to angles less than 30° (dotted blue line, Figure 4a). These intensity values (for $\phi = 0$) are extended over the surface of a sphere of radius $75D_j$ by assuming axisymmetric propagation.

[30] Because the surface area elements are larger toward the equator of the sphere, the power contributions associated with the acoustic energy flux through $\Delta S(\theta_l)$ differ from the intensity values (Figure 4b). The resulting acoustic power,

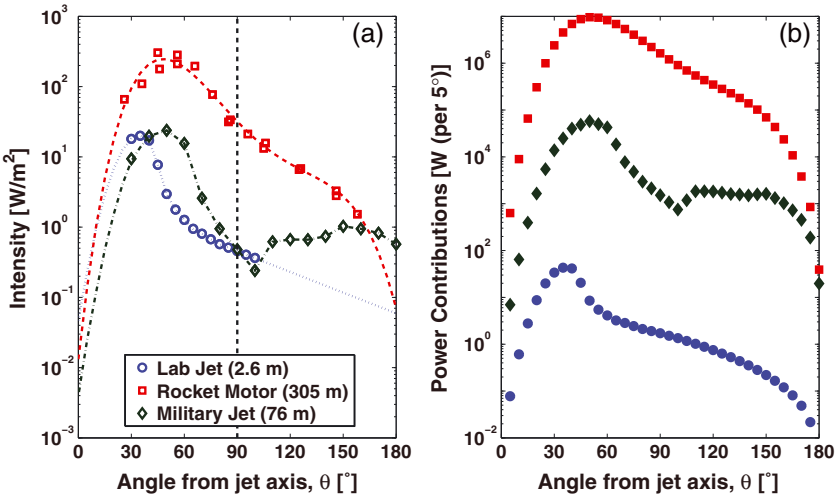


**Figure 4.** Directionality of noise from a laboratory-scale jet (blue circles), a full-scale military jet aircraft (green diamonds), and a full-scale rocket motor (RSRM) (red squares). (a) Intensity for the Mach 2.0, unheated laboratory jet at a distance of 2.6 m ($75D_j$); for the military jet at a distance of 76 m ($\sim 89D_j$); and for the rocket motor at a distance of 305 m ($\sim 80D_j$). The dip in intensity for the military jet at around 100° is due to shielding from the aircraft. (b) Estimated radiated power per 5° increment on the surface of a sphere with the radius indicated in the legend: $\overline{\Pi}_l = \bar{I}(\theta_l)\Delta S(\theta_l)$.

**Table 1.** Acoustic Power Estimates for Various Jet Flows Taking Into Account the Measured Directionality Compared to Estimates Based Only on the Acoustic Intensity at 90° From the Jet Axis[a]

| | $\overline{\Pi}$ Over a Sphere (W) | | | $\overline{\Pi}$ Over a Hemisphere (W) | | |
|---|---|---|---|---|---|---|
| Jet | $\overline{\Pi}_{ALL} = \sum \bar{I} \Delta S$ | $\overline{\Pi}_{90} = 4\pi r^2 \bar{I}_{90}$ | % Error | $\overline{\Pi}_{ALL} = \sum \bar{I} \Delta S$ | $\overline{\Pi}_{90} = 2\pi r^2 \bar{I}_{90}$ | % Error |
| Lab-scale | 213 W | 39.3 W | 82% | 203 W | 19.7 W | 90% |
| ($r$ = 2.6 m) | (143 dB) | (136 dB) | | (143 dB) | (133 dB) | |
| Military aircraft | $3.45 \times 10^5$ W | $3.47 \times 10^4$ W | 90% | $3.23 \times 10^5$ W | $1.74 \times 10^4$ W | 95% |
| ($r$ = 76 m) | (175 dB) | (165 dB) | | (175 dB) | (162 dB) | |
| Rocket motor | $7.95 \times 10^7$ W | $3.73 \times 10^7$ W | 53% | $7.42 \times 10^7$ W | $1.86 \times 10^7$ W | 75% |
| ($r$ = 305 m) | (199 dB) | (196 dB) | | (199 dB) | (193 dB) | |
| Tungurahua | $3.2 \times 10^7$ to $1.6 \times 10^8$ W[b] | $1.6 \times 10^7$ W | *50–90*[b]% | $3.2 \times 10^7$ to $1.6 \times 10^8$ W[b] | $8.1 \times 10^6$ W | 75–95[b]% |
| ($r$ = 36.8 km) | (195 to 202 dB)[b] | (192.1 dB) | | (195 to 202 dB)[b] | (189.1 dB) | |

[a]We compare estimates assuming both a sphere and a hemisphere of radius $r$ (see text for details). The overall power level in dB (re 1 pW) is given in parentheses.

[b]These values for Tungurahua volcano are inferred by assuming the same range in % error as obtained for the other jet sources and are provided simply for discussion.

computed using equation (12) for $\overline{\Pi}$, is 213 W (OAPWL = 143 dB) (Table 1).

[31] To make this example more similar to a volcano, we now restrict the angles from the jet axis to the upper half plane (angles less than vertical dashed line in Figure 4a), assuming now that the jet is pointing in the upward direction ($z > 0$). The resulting acoustic power is 203 W (143 dB) (Table 1). The power value that results from including only $\theta \leq 90°$ is not significantly different from when all angles are included because the power contributions at the large values of $\theta$ are considerably less than those closer to the exhaust axis (Figure 4b).

### 3.3. Reusable Solid Rocket Motor and Military Jet

[32] A solid rocket motor is a man-made jet noise source that is perhaps more analogous to a volcanic jet than the laboratory-scale jet. Unlike the laboratory-scale jet discussed in section 3.2, the exhaust of a solid rocket motor is a high-temperature, multiphase jet. Recently, NASA funded acoustics measurements from three static reusable solid rocket motor (RSRM) firings at ATK Space Systems in Promontory, UT [*Kenny et al.*, 2009]. The four-segment RSRMs were those used in the NASA Space Shuttle. The RSRMs were fired horizontally toward a hillside at ATK in northern Utah [*Kenny et al.*, 2009]. Data were collected using Bruel and Kjaer 6.35 mm pressure microphones at sampling rates of 48 and 96 kHz. The microphones were placed along an arc of radius 305 m (1000 ft), which is approximately $80D_j$ (Figure 3). Jet velocity information is not available for the rocket motor data.

[33] Figure 4a shows the acoustic intensity as a function of angle along the $80D_j$ arc between 50–60 s during the ~120 s rocket motor burn [*Gee et al.*, 2013]. The greatest variation of intensity values between firings occurs in the region of maximum intensity at 45–70°. We use a polynomial fit to the intensity (dashed red line, Figure 4a) for the calculations because of the spread in the data between firings and to extrapolate the function an extra 20° on either side of the measurement aperture.

[34] Similar to the method used for the laboratory jet, we extend the intensity in Figure 4a for the rocket over the surface of a sphere and hemisphere of radius 305 m (1000 ft) to calculate acoustic power (Table 1). For the rocket, the acoustic power over the sphere is $7.95 \times 10^7$ W (199 dB), whereas over the hemisphere it is $7.42 \times 10^7$ W (199 dB) (Table 1).

[35] We follow the same procedure for data recorded at 76 m (250 ft, approximately $89D_j$) from a high-performance military jet aircraft operating at military power [*Gee et al.*, 2012]. The data are from a tie-down test in which the jet exhaust flow is horizontal. Jet velocity information is not available for the military aircraft data. The green dashed-dotted line in Figure 4a is a linear interpolation through the data points from 30 to 180° and a polynomial fit from 0 to 30° degrees based on the 30–50° data points. For the military aircraft, the acoustic power over the sphere is $3.45 \times 10^5$ W (175 dB), whereas for the hemisphere it is $3.23 \times 10^5$ W (175 dB) (Table 1). Similar to the lab-scale jet and the solid rocket motor, when the directionality of the jet noise is accounted for, there is little difference between the power radiated over a sphere versus a hemisphere because the dominant power contributions are from angles close to the jet exhaust.

[36] We note that for the military aircraft and rocket data, the measurement conditions are not ideal. Because these experiments were conducted outdoors and not in an anechoic chamber, the ground surface likely affects signal amplitudes via ground reflections. Furthermore, there is the possibility that additional solid-fluid turbulent interactions occurred between the rocket exhaust jet flow and the solid ground surface. This is more likely for the rocket motor exhaust than for the military jet exhaust, because the rocket motor exhaust impinged more on the ground surface. While important to note, these complications do not significantly affect the conclusions and recommendations of this study.

### 3.4. Comparison With Spherical Spreading Assumption

[37] We now determine the value of acoustic power obtained by assuming spherical spreading from a single microphone measurement (i.e., neglecting all source directionality); this assumption has been used in numerous volcano acoustics studies [e.g., *Woulff and McGetchin*, 1976; *Vergniolle and Caplan-Auerbach*, 2006; *Caplan-Auerbach et al.*, 2010; *Delle Donne and Ripepe*, 2012; *Ripepe et al.*, 2013]. While this may be a reasonable approximation for a relatively compact strombolian explosion, it will be inac-

curate for a large extended subplinian or plinian jet. If a single measurement is chosen to represent all of the $\bar{I}(\theta_l)$ in the summation for $\overline{\Pi}$ (equation (13)), the assumption is being made that a monopole is radiating at the origin. Factors of $4\pi r^2$ for a sphere and $2\pi r^2$ for a hemisphere could then be used in place of the summation and the factors of $\Delta S(\theta_l)$ (equation (13)). If this monopole assumption is made, a significantly different value is obtained for the acoustic power.

[38] As an example, we predict the acoustic power values that would be obtained assuming spherical spreading with the laboratory-scale jet (section 3.2). Using the sideline ($\theta$ = 90°) measurement of the mean-square pressure, the acoustic power calculation yields 39.3 W (136 dB) for a sphere and 19.7 W (133 dB) for a hemisphere (Table 1).

[39] In Table 1, we show the results of similar calculations for the rocket and military jet aircraft. The columns labeled "$\overline{\Pi}_{\mathrm{ALL}}$" contain the power calculated with the method described in sections 3.1–3.3, namely by numerically approximating the integral of the intensity over the surface (equation (13)). The columns labeled "$\overline{\Pi}_{90}$" show the acoustic power obtained by using a monopole assumption with spherical spreading and the acoustic intensity at 90° (sideline). In Table 1, we also report the % error calculated from

$$\%\ \text{error} = 100\frac{\overline{\Pi}_{\mathrm{ALL}} - \overline{\Pi}_{90}}{\overline{\Pi}_{\mathrm{ALL}}}. \tag{15}$$

It is important to note that the 90° case can underestimate the acoustic power by about 50 to 95% (Table 1).

[40] This leads to the important question of how much the acoustic power of a volcanic jet is underestimated by assuming spherical spreading and using data from limited infrasound measurement locations. Although difficult to answer without sampling the full directionality of volcanic jet noise, we make an estimate based on the % errors obtained for the other jet sources (Table 1). The final row in Table 1 shows $\overline{\Pi}_{90}$ values estimated for an infrasound signal from an eruption on 14–15 July 2006 at Tungurahua Volcano, Ecuador (see section 4 for more details). The infrasound data are collected at a distance of $r$ = 36.75 km from the source, and the angle between the vent at 5 km altitude and station at 2 km altitude is about 94.6°, which we take to be ~90° (Figure 3) [*Matoza et al.*, 2009a; *Fee et al.*, 2010a].

[41] The $\overline{\Pi}_{90}$ value is estimated by assuming spherical spreading over the entire sphere ($\overline{\Pi}_{90} = \overline{\Pi}_{\mathrm{sph}}$) or a hemisphere ($\overline{\Pi}_{90} = \overline{\Pi}_{\mathrm{hem}}$) (Appendix A), even though we know this assumption is not valid, and by additionally assuming that $\rho_0$ = 1.2 kg/m$^3$ and $c$ = 330 m/s. The values of $\overline{\Pi}_{90}$ reported in Table 1 correspond to the maximum 5 min intensity values measured during the eruption (see section 4). We then scale the values of $\overline{\Pi}_{90}$ into an estimate of $\overline{\Pi}_{\mathrm{ALL}}$ by assuming 50–90% underestimation for the spherical spreading assumption, and 75–95% underestimation for the hemispherical assumption, which cover the ranges obtained for the other jet sources; we report these estimates in the last row of Table 1. We note, however, that the % errors are likely to vary with jet velocity (Mach number) and other factors and these examples should therefore be taken only as an illustration of potential errors in this approach for estimating acoustic power. The % error values in Table 1 are unlikely to be generally applicable for converting $\overline{\Pi}_{\mathrm{sph}}$ estimates into $\overline{\Pi}_{\mathrm{ALL}}$, and should not be used this way in future work.

[42] While there are logistical limitations on the available microphone measurement locations in field studies of military jets, rockets, and volcanoes (Figure 2b), the variation in these estimates of acoustic power (Table 1) clearly indicates that a decent representation of the jet noise directionality is needed to make reliable acoustic power estimates. This has important implications when considering acoustic power $\overline{\Pi}$ versus jet velocity scaling laws of the forms in equations (2)–(3). Given the logistical considerations of most volcano acoustics experiments, we conclude that $\overline{\Pi}$ is very difficult to estimate reliably for volcanic jets. Therefore, scaling laws in terms of acoustic power cannot be used. Typical volcano acoustics measurements, which have limited angular sampling of jet noise directionality, better represent point measurements of acoustic intensity $\bar{I}(\theta)$ rather than acoustic power. In section 4, we show that the scaling laws describing the velocity dependence for acoustic intensity are different from those for acoustic power.

## 4. Velocity Dependence of Jet Noise

[43] The acoustic power versus gas exit velocity scaling laws used in previous volcano acoustics studies (equations (2)–(3)) are largely outdated and have been replaced with new scaling laws that take into account factors such as observation angle and temperature. In sections 1 and 2.4, we introduced the acoustic power versus gas exit velocity scaling laws used by *Woulff and McGetchin* [1976] (equations (2)–(3)), which were from early acoustic analogy theory. These results did not take into account jet noise directionality. Even from the point of view of acoustic analogy theory, the study by *Woulff and McGetchin* [1976] is outdated. *Woulff and McGetchin* [1976] state that jet noise without a solid boundary is purely quadrupole and this does not reflect later research based on the acoustic analogy [e.g., *Lilley*, 1991] that suggested that jet noise free from boundaries could contain dipole and monopole contributions as well. As reviewed by *Viswanathan* [2006, 2009], later research using acoustic analogy theory provided different formulations and more general scaling laws for heated jets of the form

$$\bar{I}(\theta = 90°) \propto A'\left(\frac{V_j}{c}\right)^8 + B'\left(\frac{V_j}{c}\right)^6 + C'\left(\frac{V_j}{c}\right)^4, \tag{16}$$

where $\bar{I}(\theta = 90°)$ is the acoustic intensity radiated at an angle 90° from the jet axis (see Figure 2a); and $A'$, $B'$, and $C'$ are complex functions of the temperature ratio ($T_t/T_0$, where $T_t$ is the stagnation or reservoir temperature, and $T_0$ is the ambient temperature). The right-hand side of equation (16) can be recognized as a multipole addition of the three basic sources in equations (2)–(3). Note, however, that this formulation with fixed integer exponent values of 4, 6, and 8 (i.e., monopoles, dipoles, and quadrupoles) has subsequently been abandoned (section 2.3). In this section, we highlight the new scaling laws proposed by *Viswanathan* [2004, 2006, 2009] and discuss their implications for volcano acoustics.

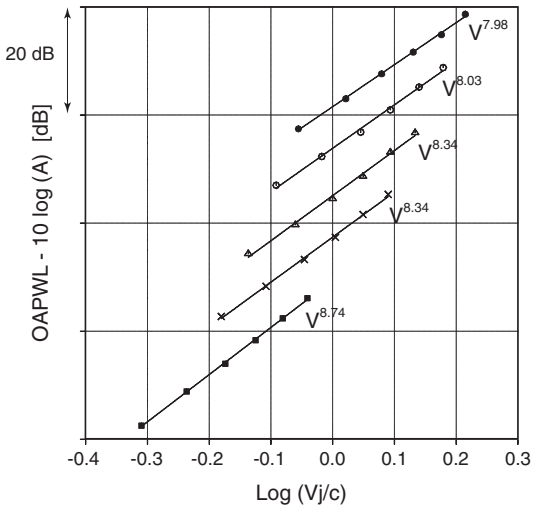


**Figure 5.** Variation of OAPWL with jet velocity for jets with various temperature ratios: $T_t/T_0$ = 1.0 (black squares); $T_t/T_0$ = 1.8 (crosses), $T_t/T_0$ = 2.2 (triangles); $T_t/T_0$ = 2.7 (open circles); $T_t/T_0$ = 3.2 (filled circles). Jet velocity is expressed as a ratio with respect to the ambient sound speed $c$. The jet diameter is 2.45 inches and OAPWL has been corrected for jet nozzle exit area $A$ by $10\log(A)$. The labels indicate the velocity power law dependence $V^n$ for each case. The abscissa corresponds to a Mach number ($V_j/c$) ranging from ∼0.4 to 2. This figure represents a relatively small range of Mach number. The approximately $V^8$ relation obeyed for these data is known to break down at higher Mach numbers toward a $V^3$ dependence. Figure is reproduced from *Viswanathan* [2004, 2006] and used with permission.

### 4.1. New Scaling Laws Based on Experimental Data

[44] Laboratory experiments indicate that the acoustic power dependence on jet velocity does closely approximate Lighthill's $V^8$ law for a small range of Mach number [e.g., *Viswanathan*, 2006; *Tam et al.*, 2008; *Viswanathan*, 2009], however, with weak additional dependence on the temperature ratio [*Viswanathan*, 2004, 2006]

$$\overline{\Pi} \propto \left(\frac{V_j}{c}\right)^n, \tag{17}$$

$$n = n\left(\frac{T_t}{T_0}\right). \tag{18}$$

As shown in Figure 5, the exponent $n$ in the acoustic power with jet velocity scaling law (equations (17), (18)) is close to, but not exactly, 8. The $V^8$ power law is known to break down at higher Mach number [e.g., *Chobotov and Powell*, 1957; *Howes*, 1960; *Ffowcs Williams*, 1963; *Schlinker et al.*, 2007], a fact pointed out by *Woulff and McGetchin* [1976]. For rockets, the acoustic power dependence on jet velocity is found to approximate $V^3$ [*Chobotov and Powell*, 1957; *Eldred*, 1971].

[45] However, the exponents in the acoustic intensity dependence on jet velocity are much more variable than those for acoustic power [*Viswanathan*, 2006]

$$\bar{I}(\theta) \propto \left(\frac{V_j}{c}\right)^{n_\theta}, \tag{19}$$

$$n_\theta = n\left(\theta, \frac{T_t}{T_0}\right). \tag{20}$$

The exponent $n_\theta$ in this case (equations (19) and (20)) is a function not only of the temperature ratio but also of the observation angle $\theta$ (the angle from the jet axis, see Figure 2). The dependence on observation angle $\theta$ is very strong (Figure 6), reflecting the highly directional nature of jet noise. Note in Figure 6 that the exponent $n_\theta$ varies nonlinearly between ∼5 and 10 as a function of temperature ratio and observation angle. This extreme variability in power law exponent has major implications for the use of such scaling laws to understand infrasonic signals from volcanic eruptions. In stark contrast to the scaling laws used by *Woulff and McGetchin* [1976], where $n$ takes only integer values of 4, 6, or 8 (equations (2)–(3) and (8)), $n_\theta$ in equation (20) varies smoothly between ∼5 and 10.

[46] It is important to note that these scaling laws (equations (17)–(20)) were derived from laboratory measurements of pure-air jet flows [*Viswanathan*, 2006]. Volcanic jet flows are likely to deviate significantly from the pure-air case (see section 5). Thus, we may reasonably conclude that $n$ (equation (18)) and $n_\theta$ (equation (20)) are not yet known for volcanic jet flows and that Figure 6 would differ significantly for the volcanic case because of additional complexities and unknowns in volcanic jet flows (see section 5). We also note that the results of *Viswanathan* [2006] shown in Figure 6 are for a relatively limited Mach number range, and the exponents $n_\theta$ are expected to change

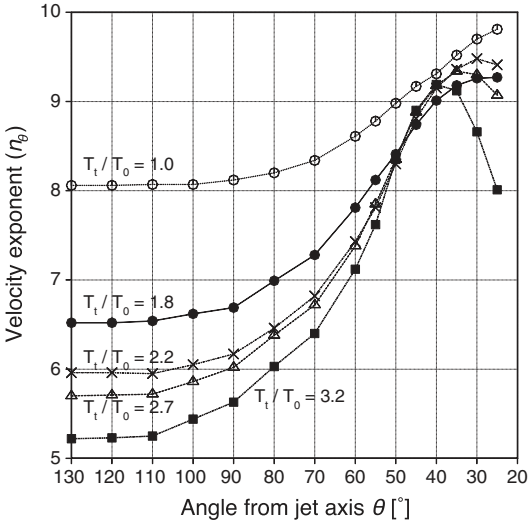


**Figure 6.** Variation of the velocity exponent $n_\theta$ in equations (19) and (20) with angle from the jet axis $\theta$ for pure-air jet flows. This figure, produced using a high-quality laboratory jet noise database, illustrates the strong variability in observed power law exponent $n_\theta$ due to jet noise directionality. Different curves correspond to different values of temperature ratio $T_t/T_0$, where $T_t$ is the stagnation or reservoir temperature and $T_0$ is the ambient temperature. Note that the crossover point between LST and FST dominance occurs at different $\theta$ for different temperature ratios. Figure is reproduced from *Viswanathan* [2006] and used with permission.

with increasing Mach number [see Figure 7 in the paper by *Schlinker et al.*, 2007].

### 4.2. Implications of the New Scaling Laws

[47] In this section, we discuss the implications of sections 3–4.1 for methods used to solve for gas exit velocity and other quantities that depend on gas exit velocity [e.g., *Vergniolle and Caplan-Auerbach*, 2006; *Caplan-Auerbach et al.*, 2010; *Delle Donne and Ripepe*, 2012; *Ripepe et al.*, 2013]. Rearranging equation (8), we obtain

$$V_j = \left( \frac{\overline{\Pi}}{c^{3-n} K \rho_0 A_v} \right)^{\frac{1}{n}}. \quad (21)$$

Based upon sections 3–4.1, we contend that the empirical constant $K$ and exponent $n$ are largely unknown for volcanic jets. Values of $K_D = 10^{-2}$ and $K_Q = 10^{-5}$ (equations (3) and (3)) were proposed by *Woulff and McGetchin* [1976]. The value of $K_D = 10^{-2}$ originated from experiments on the idealized case of jet flow past a taut wire [*Leehey and Hanson*, 1971], while the value of $K_Q = 10^{-5}$ originated from early jet noise experiments. However, $K$ is not a universal constant and is likely to vary strongly with factors such as tephra loading, nozzle geometry, etc.

[48] In section 3, we showed that $\overline{\Pi}$ is difficult to estimate reliably unless there is good angular sampling of the jet directionality; this is not usually possible for volcanic jets. Because volcano acoustic field experiments therefore represent point measurements of $\bar{I}(\theta)$ rather than $\overline{\Pi}$, the pertinent exponent is actually $n_\theta$ (equation 19), which is highly variable (Figure 6). When using $\overline{\Pi}_{sph}$ as an estimate of $\overline{\Pi}$, as done by *Woulff and McGetchin* [1976], the distinction between $n$ and $n_\theta$ becomes unclear.

[49] Previous studies have investigated the suitability of the scaling laws proposed by *Woulff and McGetchin* [1976] using infrasound data combined with other data used to infer gas exit velocity. For example, *Caplan-Auerbach et al*. [2010] found that a good fit to plume height data was obtained by using equation (3), i.e., a dipole source with $n = 6$. Similarly, *Ripepe et al.* [2013] investigated the same scaling laws and again found that a dipole source ($n = 6$) results in the best fit with velocities derived from thermal camera imagery. However, the scaling laws of *Woulff and McGetchin* [1976] only allow for integer values of $n = 4$, 6, or 8, and we propose that a larger range of (non-integer) values could be explored in future work.

[50] To summarize, the following issues with equation (21) are identified based on sections 3–4.1:

[51] 1. Jet noise is directional and therefore isotropic radiation cannot be assumed. For this reason, typical volcano acoustics source-receiver geometries do not measure $\overline{\Pi}$ for volcanic jets; they measure $\bar{I}(\theta)$.

[52] 2. The exponents $n_\theta$ in the velocity dependence for $\bar{I}(\theta)$ (∼5–10 for pure-air jets, unknown for volcanic jets) are different from the exponents $n$ in the relations for $\overline{\Pi}$.

[53] 3. $\overline{\Pi}_{sph}$ is a poor approximation to $\overline{\Pi}$ for two reasons:

a. $\overline{\Pi}_{sph}$ systematically underestimates $\overline{\Pi}$ for a fixed (steady state) value of velocity.

b. $\overline{\Pi}_{sph}$ does not have the same velocity dependence as $\overline{\Pi}$. Because $\overline{\Pi}_{sph}$ is linearly related to $\bar{I}(\theta)$ (equation (11)), the exponents in $\overline{\Pi}_{sph}$ will be similar to those for $\bar{I}(\theta)$ (∼5–10 for pure-air jets, unknown for volcanic jets).

[54] 4. The acoustic power coefficients $K$ are unknown for volcanic jets.

[55] 5. Poor constraints on $n$, $n_\theta$, and $K$ propagate into poor constraints on $V_j$.

[56] We illustrate these issues with an example, which is intended as a caution about using equation (21) to infer $V_j$. We take data recorded from the 14–15 July 2006 eruption of Tungurhua Volcano, Ecuador (Figure 7a) (also used in section 3.4). The data are from the RIOE infrasound array, 36.75 km from Tungurahua and sampled at 40 Hz [*Matoza et al.*, 2009a; *Fee et al.*, 2010a]. We only consider signal that has been identified by array processing as originating from the volcano. We estimate the mean-square pressure $\overline{p^2}$ in 5 min time windows (Figure 7b). Following *Woulff and McGetchin* [1976], we then assume a spherical source and recover $\overline{\Pi}_{sph}$ from equation (11), even though we know that this is not a valid assumption because we have not captured the jet noise directionality (points 1 and 3a, above) (Figure 7c). In addition, we allow $n$ to vary by as much as $n_\theta$ to account for the ambiguity associated with the assumption of isotropic radiation (points 2 and 3b, above).

[57] We assume the following parameters: $\rho_0 = 1.2$ kg/m$^3$, $c = 330$ m/s, source (jet) radius = 150 m, and $r = 36.75$ km [*Matoza et al.*, 2009a]. In Figure 7d, we show the effect of additionally assuming that $K = 10^{-2}$ and $n = 6$ [these are the best-fit values obtained by *Caplan-Auerbach et al.*, 2010; *Ripepe et al.*, 2013]. Because $\overline{p^2}$ gradually increases with time during this eruption (Figure 7a), the inferred $V_j$ (Figure 7d) also increases. Based on these assumptions, the jet velocity $V_j$ ranges from 52 m/s to 94 m/s during the eruption ($V_{max} = 94$ m/s, $V_{range} = 42$ m/s).

[58] We now repeat these steps, using values of $K$ ranging from $10^{-6}$ to $10^{-1}$ and values of $n$ ranging from 5 to 10. We have deliberately chosen a very wide range in $K$, because we contend that $K$ is not constrained for volcanic jets (point 4, above). Nevertheless, the range covers the values of $10^{-5}$ to $10^{-2}$ proposed by *Woulff and McGetchin* [1976]. We report the range in implied velocities $V_{range}$ and the maximum inferred velocity $V_{max}$ for different values of $n$ and $K$ (Figures 7e and 7f). Figures 7e and 7f show that the effect of unknown $K$ and $n$ leads to large uncertainty in the values of inferred jet velocity (point 5, above). Indeed, based on our chosen range in values of $K$ and $n$, the implied maximum jet velocity $V_{max}$ could be anything from ∼50 m/s to 450 m/s. This is a large range in velocities that spans subsonic and supersonic values relative to the ambient sound speed, with widely different implications for eruption column scenarios that would result from a volcanic jet with this velocity.

## 5. Discussion

[59] The infrasound produced by volcanic jet flows is in some ways similar, but is not perfectly analogous, to the jet noise produced by smaller scale man-made jets [*Matoza et*

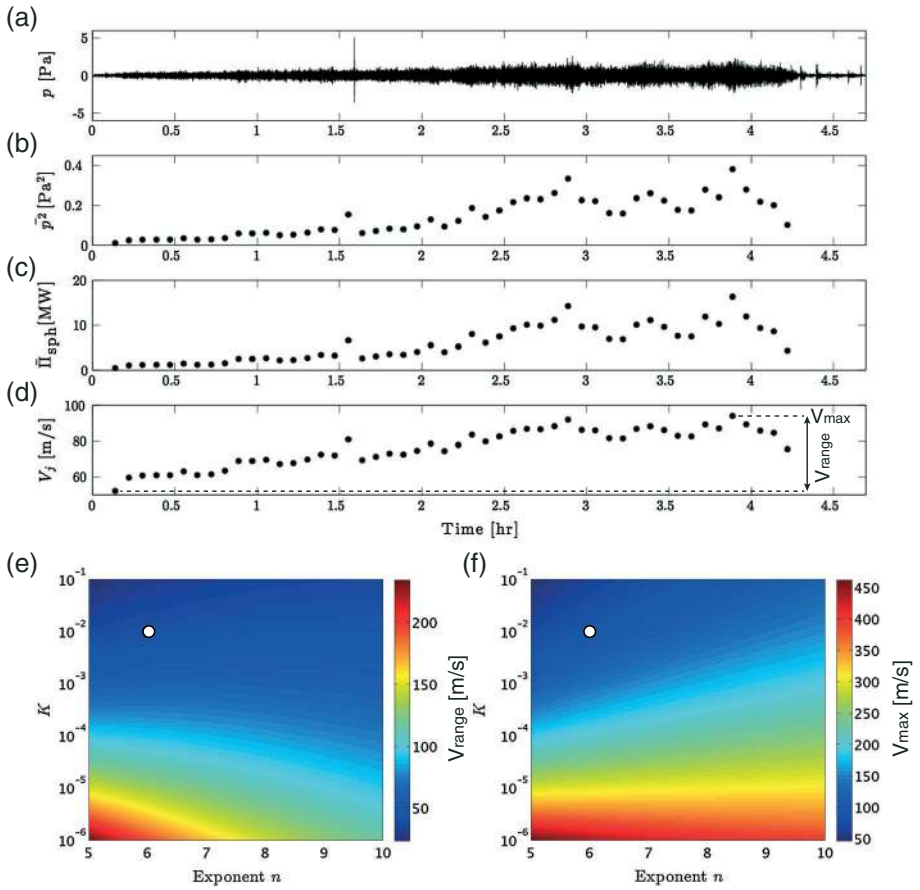


**Figure 7.** Application of equation (21) to the 14–15 July 2006 Tungurahua eruption in order to illustrate the large uncertainties in $V_j$ when $K$ and $n$ are unconstrained. (a) Beamformed waveform from the RIOE array showing the eruption infrasound signal ("volcanic jet noise") with amplitude increasing with time. Plot origin time is 22:36:18 UTC, 14 July 2006. (b) Five minute mean-square pressure $\overline{p^2}$. (c) Acoustic power assuming spherical spreading $\overline{\Pi}_{sph}$; this assumption is not valid. (d) Inferred jet velocity $V_j$ from equation (21) assuming $\rho_0 = 1.2$ kg/m$^3$, $c = 330$ m/s, source (jet) radius = 150 m, $r = 36.75$ km, $K = 10^{-2}$, and $n = 6$. Based on these assumptions, $V_j$ ranges from 52 m/s to 94 m/s ($V_{max} = 94$ m/s, $V_{range} = 42$ m/s). We then assess how (e) $V_{range}$ and (f) $V_{max}$ (see Figure 7d) vary as a function of different trial values of $n$ and $K$, while keeping all other parameters held fixed. White circles indicate values of $K = 10^{-2}$ and $n = 6$ used in Figure 7d. Because, e.g., $K$ and $n$ are currently unconstrained for a volcano, a very wide range of different velocities can be inferred (jet velocity is poorly constrained).

*al.*, 2009a]. In volcano acoustics, we want to know the velocity and angular dependence of an exotic jet noise source. Volcanic jet noise is likely to deviate from the pure-air man-made case because of complexities such as multiphase flow (especially loading with tephra particles); interaction with the shallow conduit structure and vent walls; nozzle (vent) geometry and roughness; complex and dynamic crater morphology (e.g., volcanic jet eroding a vent and/or crater); buoyancy effects; and high temperature and density effects. An additional complication is that the internal sound speeds for volcanic jets [e.g., *Kieffer and Sturtevant*, 1984] are different from the internal sound speeds in jets that have previously been studied, e.g., pure-air laboratory jets and exhausts of jet aircraft and rockets. Therefore, in the case of volcanic jets, the combination of the Mach number with respect to the ambient sound speed and the Mach number with respect to the fluid composing the jet (called the exhaust Mach number) is likely different from any jet noise source that has previously been studied. The exponents (equation (20)) are not yet characterized for a solid rocket motor, much less for a volcanic jet.

[60] We note that even for pure-air jet flows, a first-principles noise prediction theory is far from complete [*Tam*, 1998; *Tam et al.*, 2008]. Advances have been made in aeroacoustics research based upon detailed empirical data. Advances have also been made with numerical simulations of jet noise, although major computational challenges remain to be addressed [*Bailly and Bogey*, 2004; *Tam*, 2004; *Wang et al.*, 2006; *Bodony and Lele*, 2008].

[61] We have emphasized that in volcano acoustics field experiments, we are generally confined to upstream observation angles ($\theta > 90°$), such that sampling the directionality of volcanic jet noise is limited or impossible (Figures 2 and 3). Figure 8 illustrates the sound propagation from Tungurahua Volcano to the RIOE array 36.75 km away. Similar to Figure 2b, Figure 8 shows that rays arriving from the

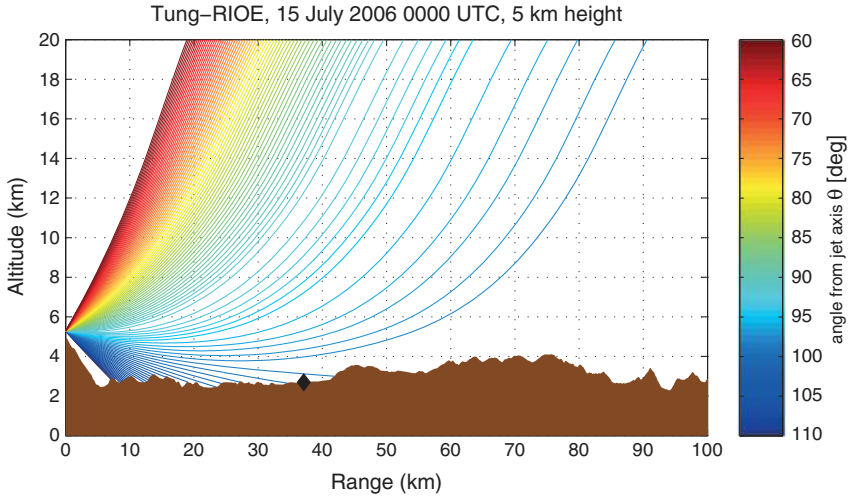


**Figure 8.** Ray-tracing simulation of acoustic propagation from Tungurahua to the RIOE array (black diamond) at 0000 UTC 15 July 2006 for a source at 5 km elevation (vent altitude) using G2S atmospheric specifications [*Drob et al.*, 2003]. Rays are launched at angles $60° \leq \theta \leq 110°$ (color scale), where $\theta$ is the angle from the jet axis. Rays terminate when they intersect the ground-surface topography (brown shaded profile). The line-of-sight angle $\theta$ between the vent (5 km elevation) and RIOE (2 km elevation, 37 km range) is about 94.6°, whereas $\theta$ for the eigenray connecting source to receiver is about 97.5°.

upstream direction of the jet ($\theta > 90°$) are recorded at RIOE, whereas rays in the downstream direction propagate upward into the atmosphere and are not recorded by the local array. *Matoza et al.* [2009a] showed that the infrasound signals associated with sustained explosive eruptions at Tungurahua and Mount St. Helens resemble the spectrum of large-scale-turbulence (LST) mixing noise more than that of fine-scale turbulence (FST) mixing noise. This is not consistent with the directionality of jet noise characterized in laboratory experiments with pure-air jets (Figure 2a), which indicate that LST noise is dominant in the downstream direction of the jet ($\theta < 55°$; the crossover angle varies with jet conditions) [*Tam*, 1998]. This observation further emphasizes the need to characterize and understand the directionality of volcanic jet noise sources before we can make quantitative inferences about jet velocity from acoustic intensity or power. This also highlights the preliminary nature of the comparison between volcanic infrasound and jet noise source processes [*Matoza et al.*, 2009a] and shows that much more work is required to test the applicability of the LST noise generation mechanism to volcanic jets.

[62] In Figure 8, the takeoff angle with respect to the jet axis ($\theta$) is 97.5° for the eigenray, defined as the ray connecting the source at 5 km elevation and RIOE. Because Figure 8 represents atmospheric conditions for a single specific time (0000 UTC 15 July 2006), we further investigated the variability in eigenray takeoff angle. We launched separate simulations for example days from each season, running four simulations for each day at 6 hr sampling intervals (16 simulations total). We found that the eigenray takeoff angle changed by less than 3° in these simulations, indicating very minor variability in jet directionality sampling as a function of atmospheric conditions at this source-receiver range. However, as shown in Figure 8, the RIOE array is located near the beginning of the shadow zone, where propagation effects on acoustic intensity values can be significant [*Fee and Garces*, 2007].

[63] In section 3, the assumption was made that at a certain distance (i.e., in the far-field), the extended jet noise source (Figure 2) can be treated as compact with sound radiating radially from a point source. Such a far-field distance would also exist for a volcanic jet flow if it were radiating into a homogeneous atmosphere. In reality, the length scale of the volcanic radiation pattern likely approaches those of atmospheric wind and temperature gradients that control infrasonic propagation [see, e.g., *Le Pichon et al.*, 2010]. In this case, sound is refracted and ducted in various waveguides before reaching the distance at which a far-field assumption is valid. Thus, as shown in Figure 8, noise from small $\theta$ angles is radiated to elsewhere in the atmosphere and does not contribute to the wave field recorded horizontally from the source, such that a compact point source assumption cannot be used.

[64] Throughout this paper, we have argued that the relations between volcanic gas exit velocity $V$ and acoustic power $\overline{\Pi}$ proposed by *Woulff and McGetchin* [1976] are likely inaccurate for infrasound signals from volcanic eruptions. Instead, relations involving acoustic intensity may be more appropriate. *Tam* [2006] and *Tam et al.* [2008] provided a dimensional analysis of jet noise data, with similar conclusions to those of *Viswanathan* [2006, 2007] (equation (19)). *Tam* [2006] expressed the relationship in equation (19) in a non-dimensional form

$$\frac{\overline{p^2}(r,\theta)}{p_0^2} = A\frac{\left(\frac{V_j}{c}\right)^{n\theta}}{\left(\frac{r}{D_j}\right)^2}, \tag{22}$$

where $n_\theta$ and the proportionality factor $A$ are both functions of $\theta$ and the temperature ratio $T_t/T_0$. We note that *Tam* [2006] interchanges the mean-square pressure $\overline{p^2}$ with a loose "acoustic intensity", by dropping the constant factor of $\rho_0 c$, which we do not follow here. Geometrical spreading $(1/r^2)$ is included by the denominator $(r/D_j)^2$.

[65] Pure-air laboratory jet noise data can be described by the form in equation (22) [*Tam*, 2006]. Based on these results, the existence of a scaling law with a similar form to equation (22) seems promising for volcanic jets. For volcanic jets, we may expect $n_\theta$ and $A$ to depend on, e.g., density, tephra particle loading, and other factors discussed above, in addition to the temperature and angular dependence observed for pure-air jets. Detailed field measurements and numerical and laboratory studies are necessary to determine the functional dependence of $A$ and $n_\theta$ on volcanic jet parameters. This work can build upon the studies of *Caplan-Auerbach et al.* [2010], *Delle Donne and Ripepe* [2012], and *Ripepe et al.* [2013], which investigated the previous scaling laws of *Woulff and McGetchin* [1976]. It is important to constrain the functional dependence of acoustic intensity or power on volcanic jet velocity because incorrect estimates of eruption velocity will propagate into predictions of, e.g., plume altitude and mass eruption rate.

[66] Regarding future directions of this work, we envision that field studies correlating infrasound data with, e.g., high-speed imaging techniques will enable relationships between acoustic intensity and gas exit velocity to be determined empirically [see, e.g., *Gerst et al.*, 2008; *Marchetti et al.*, 2009; *Taddeucci et al.*, 2012; *Delle Donne and Ripepe*, 2012; *Gerst et al.*, 2013; *Ripepe et al.*, 2013]. The form shown in equation (22) is a potential starting point. These empirical relations should be explored for a range of eruption styles. For example, it is important to differentiate sustained eruptions involving jet flows from more impulsive and discrete explosive blasts. Intermediate scenarios (e.g., discrete blasts combined with short-lived jetting) represent additional challenges that deviate further from what is characterized in aeroacoustic studies of sustained jets.

[67] Empirical relations based upon infrasound field measurements will be limited to acoustic intensity at a given angular range. However, laboratory and numerical experiments are not constrained by the same logistics. The directional properties of jet noise from conditions mimicking those found in volcanic jets could potentially be investigated in laboratory experiments (e.g., seeding with particles, jet flow through complex vent, and crater morphology). In tandem, numerical simulations could enable the full directional wave field from more complex volcanic scenarios to be investigated. The results of laboratory and numerical experiments could be compared with the data from angles that volcano acoustic field studies permit.

[68] Finally, we note that in this paper we have neglected all properties of the volcanic recording environment, such as diffraction and scattering from topography, wind, temperature, and atmospheric attenuation [*Fee and Garces*, 2007; *Matoza et al.*, 2009b; *Marcillo and Johnson*, 2010; *Kim and Lees*, 2011; *Lacanna and Ripepe*, 2013; *Fee and Matoza*, 2013]; these additional factors must also be accounted for (or justifiably neglected) in order to arrive at robust scaling relationships.

## 6. Conclusions

[69] Infrasound can provide detailed constraints on the timing, duration, and relative vigor of local and remote explosive volcanism, and has been used in prototype eruption early warning systems [e.g., *Kamo et al.*, 1994; *Garces et al.*, 2008; *Ripepe et al.*, 2009; *Fee et al.*, 2010a; *Matoza et al.*, 2011; *De Angelis et al.*, 2012; *Fee and Matoza*, 2013]. However, estimating eruption column parameters such as jet velocity and diameter, or predicting plume altitude or mass eruption rate from infrasound data, requires a quantitative relationship between the volcanic jet flow source process and the radiated infrasound. We have reevaluated, within a modern aeroacoustics framework, approaches used to infer volcanic gas exit velocity (jet velocity) from infrasound data.

[70] Previous work in volcano acoustics proposed relations between volcanic gas exit velocity $V$ and acoustic power $\overline{\Pi}$ of the form $\overline{\Pi} \sim V^n$, where $n$ is 4, 6, or 8. Because estimating acoustic power requires the integration of acoustic intensity over a surface, estimating $\overline{\Pi}$ is difficult in volcano acoustics field experiments, where observations are typically limited to angles $\theta > 90°$. We have shown, using data from a laboratory-scale jet, a military aircraft, and a solid rocket motor, that a decent sampling of jet noise directionality is necessary to obtain a reliable estimate of $\overline{\Pi}$. Therefore, in light of recent advances in aeroacoustics research, a more appropriate starting formulation is $\bar{I}(\theta) \sim (V/c)^{n_\theta}$ (see equation (22)). In equation (22), the acoustic intensity (or mean-square pressure) in a particular direction $\theta$ from the jet centerline axis depends on jet velocity via a power law whose exponent $n_\theta$ and proportionality factor $A$ are functions of $\theta$ and temperature. Because such an exotic jet noise source has not yet been explored in the laboratory or numerically, we do not know how $n_\theta$ and $A$ vary for a volcanic jet. For a volcanic jet flow, we hypothesize that $n_\theta$ and $A$ will also significantly depend upon density and tephra particle loading, etc. Constraining $n_\theta$ and $A$ in equation (22) for volcanic jet flows, and characterizing their dependence upon volcanic jet parameters, represents a new framework and a challenge for volcano acoustics. This new framework can be developed through quantitative integration of field, numerical, and laboratory studies and would lead to a more accurate relationship between volcanic infrasound and eruption column parameters.

## Appendix A: Acoustic Observations

[71] Here we review quantitative measures of sound and how they are estimated for directional and spherically symmetric sources. Our discussion follows those of *Morse and Ingard* [1968], *Lighthill* [1978], *Pierce* [1989], and *American National Standards Institute* (*ANSI*) [1994], to which the reader is referred for more details.

[72] *Acoustic energy* is the energy in a fluid associated with a sound wave. The instantaneous *acoustic intensity* vector $\mathbf{I}$ describes the rate of transport of acoustic energy

$$\mathbf{I} = p\mathbf{u}, \tag{A1}$$

where $\mathbf{u}$ is the acoustic particle velocity (m/s) and $p$ is the acoustic pressure (Pa). Intensity has units of *watts per square meter* ($\mathrm{Wm^{-2}}$). $\mathbf{I} \cdot \mathbf{n}$ is the acoustic energy flux through a unit area perpendicular to the unit normal vector $\mathbf{n}$.

[73] The acoustic power $\overline{\Pi}$ of a source is the time-averaged rate of energy flow, with units of J/s or *watts* (W). Acoustic power is evaluated as

$$\overline{\Pi} = \int_S \bar{\mathbf{I}} \cdot \mathbf{n}_{\text{out}} \, dS, \tag{A2}$$

where $\bar{\mathbf{I}}$ is the time-averaged intensity vector on the surface $S$, and $\mathbf{n}_{\text{out}}$ is the outward pointing unit normal vector on that surface.

[74] In the near field, determining the normal component of the intensity is nontrivial. In the far field, however, we can assume that the signal is propagating outward along a radial. In this case, the time-averaged radial component of intensity $\bar{I}$ is related to the mean-square pressure $\overline{p^2}$

$$\bar{I} = \frac{\overline{p^2}}{\rho_0 c}, \tag{A3}$$

where $\rho_0$ is the ambient density and $c$ is the sound speed.

[75] For a spherically symmetric wave field, such as that originating from a monopole, $\bar{\mathbf{I}}$ is in the radial direction, and there is no variation in its magnitude with angle. At a distance $r$ from the source, the power can be recovered from

$$\overline{\Pi}_{\text{sph}} = 4\pi r^2 \bar{I} = \frac{4\pi r^2 \overline{p^2}}{\rho_0 c}. \tag{A4}$$

For a symmetric source radiating as a hemisphere over a flat ground surface

$$\overline{\Pi}_{\text{hem}} = 2\pi r^2 \bar{I} = \frac{2\pi r^2 \overline{p^2}}{\rho_0 c}. \tag{A5}$$

For a directional acoustic source, $\bar{\mathbf{I}}$ varies as a function of observation angle to the source and equations (A4) and (A5) are not valid.

[76] Quantitative measures of sound commonly make use of logarithmic scales or *levels* with decibel units (dB). The sound-pressure level (SPL) or $L_p$ in a stated frequency band is defined as

$$L_p = 10 \log_{10} \left( \frac{\overline{p^2}}{p_{\text{ref}}^2} \right), \tag{A6}$$

where $p_{\text{ref}}$ is the reference pressure 20 $\mu$Pa for airborne sound, and the frequency band of the mean-square pressure $\overline{p^2}$ is stated. The overall sound pressure level (OASPL) is the SPL over the whole bandwidth of a signal.

[77] Similarly, the sound intensity level (SIL) is defined as

$$L_I = 10 \log_{10} \left( \frac{\bar{I}}{I_{\text{ref}}} \right), \tag{A7}$$

where $\bar{I}$ is the magnitude of the vector $\bar{\mathbf{I}}$ and $I_{\text{ref}}$ is the reference sound intensity $10^{-12}$ Wm$^{-2}$. For far-field measurements, equation (A3) implies that

$$L_I = 10 \log_{10} \left( \frac{\overline{p^2_{\text{overall}}}}{I_{\text{ref}} \rho_0 c} \right). \tag{A8}$$

For cases in which the ambient density and sound speed are good approximations, the SPL and the SIL are approximately equal for far-field measurements (they differ by about 0.16 dB because of how the reference pressure and intensity are defined).

[78] Finally, the overall sound power level (OAPWL) of a source is obtained by

$$\text{OAPWL} = 10 \log_{10} \left( \frac{\overline{\Pi}}{\Pi_{\text{ref}}} \right), \tag{A9}$$

where $\overline{\Pi}$ is defined as in equation (A2) and $\Pi_{\text{ref}}$ is the reference power of $10^{-12}$ W. For a spherically symmetric source, this reduces to

$$\text{OAPWL}_{\text{sph}} = \text{OASPL} + 10 \log_{10} \left( 4\pi r^2 \right). \tag{A10}$$

However, for a directional source, OAPWL must be determined by integrating microphone measurements from a swath of angles sampling the source radiation pattern as is done in section 3. In the case of a directional source, application of equation (A10) from a single observation point leads to erroneous results.

## Notation

| | |
|---|---|
| $\rho_0$ | ambient density |
| $p_0$ | ambient pressure |
| $T_0$ | ambient temperature |
| $c$ | ambient sound speed |
| $p$ | acoustic pressure |
| $\overline{p^2}$ | mean-square pressure (bar denotes a time-averaged quantity) |
| $\rho$ | acoustic density |
| $\mathbf{u}$ | acoustic particle velocity |
| $\lambda$ | wavelength |
| $r$ | source-receiver radial distance |
| $t$ | time |
| $\dot{q}$ | source strength |
| $T_{ij}$ | Lighthill stress tensor |
| $\tau_{ij}$ | viscous stress tensor |
| $\mathbf{I}$ | acoustic intensity vector |
| $I$ | magnitude of acoustic intensity vector |
| $\bar{I}$ | radial component of acoustic intensity |
| $\overline{\Pi}$ | acoustic power |
| $\overline{\Pi}_{\text{sph}}$ | acoustic power from a spherical source |
| $\overline{\Pi}_{\text{hem}}$ | acoustic power from a hemispherical source |
| $\overline{\Pi}_{\text{ref}}$ | reference power = 1 pW |
| $I_{\text{ref}}$ | reference intensity = 1 pWm$^{-2}$ |
| $p_{\text{ref}}$ | reference pressure = 20 $\mu$Pa |
| SPL, $L_p$ | sound pressure level |
| SIL, $L_I$ | sound intensity level |
| OASPL | overall sound pressure level |
| OAPWL | overall sound power level |
| LST | large-scale turbulence |
| FST | fine-scale turbulence |
| $\mathbf{n}_{\text{out}}$ | outward pointing unit normal vector |
| $\Delta S$ | area weighting factor |
| $V$ | loosely: jet velocity or "gas exit velocity" |
| $V_j$ | fully expanded jet velocity |
| $D_j$ | fully expanded jet diameter |
| $T_t$ | stagnation temperature |
| $n$ | exponent in power law relating $V_j$ to $\overline{\Pi}$ |
| $n_\theta$ | exponent in power law relating $V_j$ to $\bar{I}(\theta)$ |
| $K$ | acoustic power coefficient |
| $A_v$ | vent area |
| $d$ | characteristic length scale |
| $\theta$ | angle from the jet axis |
| $\phi$ | polar angle around the jet axis |

[79] **Acknowledgments.** We thank Mie Ichihara and an anonymous reviewer for their careful and constructive reviews. Robin Matoza gratefully acknowledges support from the Cecil H. and Ida M. Green Foundation at the Institute of Geophysics and Planetary Physics, Scripps Institution of Oceanography. This work was also supported by NSF grants EAR-1113294 and EAR-1113338 and the Geophysical Institute of the University of Alaska, Fairbanks.

## References

ANSI (1994), American National Standard Acoustical Terminology. American National Standards Institute, (ANSI S1.1-1994; ASA 111-1994).

Bailly, C., and C. Bogey (2004), Contributions of computational aeroacoustics to jet noise research and prediction, *Int. J. Comput. Fluid Dyn.*, *18*, 481–491.

Bodony, D. J., and S. K. Lele (2008), Current status of jet noise predictions using large-eddy simulation, *AIAA J.*, *46*, 364–380, doi:10.2514/1.24475.

Caplan-Auerbach, J., A. Bellesiles, and J. K. Fernandes (2010), Estimates of eruption velocity and plume height from infrasonic recordings of the 2006 eruption of Augustine Volcano, Alaska, *J. Volcanol. Geotherm. Res.*, *189*, 12–18, doi:10.1016/j.volgeores.2009.10.002.

Chobotov, V., and A. Powell (1957), On the prediction of acoustic environments from rockets, Rama-Wooldridge Corp. Rept. E.M.-7-7.

Crow, S. C., and F. H. Champagne (1971), Orderly structure in jet turbulence, *J. Fluid Mech.*, *48*, 547–591.

Curle, N. (1955), The influence of solid boundaries upon aerodynamic sound, *Proc. R. Soc. London, Ser. A*, *231*(1187), 505–514.

Dabrowa, A. L., D. N. Green, A. C. Rust, and J. C. Phillips (2011), A global study of volcanic infrasound characteristics and the potential for long-range monitoring, *Earth Planet. Sci. Lett.*, *310*, 369–379, doi:10.1016/j.epsl.2011.08.027.

De Angelis, S., D. Fee, M. Haney, and D. Schneider (2012), Detecting hidden volcanic explosions from Mt. Cleveland Volcano, Alaska with infrasound and ground-coupled airwaves, *Geophys. Res. Lett.*, *39*, L21312, doi:10.1029/2012GL053635.

Delle Donne, D., and M. Ripepe (2012), High-frame rate thermal imagery of Strombolian explosions: Implications for explosive and infrasonic source dynamcis, *J. Geophys. Res.*, *117*, B09206, doi:10.1029/2011JB008987.

Drob, D. P., J. M. Picone, and M. Garces (2003), Global morphology of infrasound propagation, *J. Geophys. Res.*, *108*(D21), 4680, doi:10.1029/2002JD003307.

Eldred, K. M. (1971), Acoustic loads generated by the propulsion system, NASA Space Vehicle Design Criteria (Structures), NASA SP-8072, Washington, DC, United States.

Evers, L. G., and H. W. Haak (2010), The characteristics of infrasound, its propagation and some early history, in *Infrasound Monitoring for Atmospheric Studies*, edited by A. Le Pichon, E. Blanc, and A. Hauchecorne, pp. 3–27, Springer, Berlin.

Fee, D., and M. Garces (2007), Infrasonic tremor in the diffraction zone, *Geophys. Res. Lett.*, *34*, L16826, doi:10.1029/2007GL030616.

Fee, D., and R. S. Matoza (2013), An overview of volcano infrasound: From hawaiian to plinian, local to global, *J. Volcanol. Geotherm. Res.*, *249*, 123–139, doi:10.1016/j.jvolgeores.2012.09.002.

Fee, D., M. Garces, and A. Steffke (2010a), Infrasound from Tungurahua Volcano 2006–2008: Strombolian to Plinian eruptive activity, *J. Volcanol. Geotherm. Res.*, *193*, 67–81, doi:10.1016/j.jvolgeores.2010.03.006.

Fee, D., A. Steffke, and M. Garces (2010b), Characterization of the 2008 Kasatochi and Okmok eruptions using remote infrasound arrays, *J. Geophys. Res.*, *115*, D00L10, doi:10.1029/2009JD013621.

Fee, D., R. S. Matoza, K. Gee, T. Neilsen, and D. Ogden (2013), Infrasonic crackle and supersonic jet noise from the eruption of Nabro Volcano, Eritrea, *Geophys. Res. Lett.*, *40*, 4199–4203, doi:10.1002/grl.50827.

Ffowcs Williams, J. E. (1963), The noise from turbulence convected at high speed, *Philos. Trans. R. Soc. A*, *255*(1061), 469–503.

Fitzpatrick, H. M., and R. Lee (1952), *Measurements of Noise Radiated by Subsonic Air Jets*, David W. Taylor Model Basin, Navy Dept. 835, Washington, D. C.

Garces, M., D. Fee, D. McCormack, R. Servranckx, H. Bass, C. Hetzer, M. Hedlin, R. Matoza, and H. Yepes (2008), Prototype ASHE volcano monitoring system captures the acoustic fingerprint of stratospheric ash injection, *Eos Trans. AGU*, *89*, 377–379.

Garces, M. A., D. Fee, and R. S. Matoza (2013), Volcano acoustics, in *Modeling Volcanic Processes,* chap. 16, edited by S. A. Fagents et al., Cambridge Univ. Press, New York.

Gee, K. L., A. A. Atchley, L. E. Falco, M. R. Shepherd, L. S. Ukeiley, B. J. Jansen, and J. M. Seiner (2010), Bicoherence analysis of model-scale jet noise, *J. Acoust. Soc. Am.*, *128*(5), EL211–EL216.

Gee, K. L., J. M. Downing, M. M. James, R. C. McKinley, R. L. McKinley, T. B. Neilsen, and A. T. Wall (2012), Nonlinear evolution of noise from a military jet aircraft during ground run-up, *AIAA Paper*, June 2012-2258, Colorado Springs, Colo.

Gee, K. L., R. J. Kenny, T. B. Neilsen, T. W. Jerome, C. M. Hobbs, and M. M. James (2013), Spectral and statistical analysis of noise from reusable solid rocket motors, *Proc. Meetings Acoust.*, *18*, 040002.

Gerst, A., M. Hort, P. R. Kyle, and M. Voge (2008), 4D velocity of Strombolian eruptions and man-made explosions derived from multiple Doppler radar instruments, *J. Volcanol. Geotherm. Res.*, *177*, 648–660.

Gerst, A., M. Hort, R. C. Aster, J. B. Johnson, and P. R. Kyle (2013), The first second of volcanic eruptions from the Erebus volcano lava lake, Antarctica – Energies, pressures, seismology, and infrasound, *J. Geophys. Res. Solid Earth*, *118*, 3318–3340, doi:10.1002/jgrb.50234.

Howes, W. L. (1960), Similarity of far noise fields of jets, *NASA Technical Report, (NASA TR R-52).*

Hubbard, H. H. (ed.) (1991), *Aeroacoustics of Flight Vehicles: Theory and Practice*, vol. 1, Acoustical Society of America, Melville, N. Y.

Johnson, J. B. (2003), Generation and propagation of infrasonic airwaves from volcanic explosions, *J. Volcanol. Geotherm. Res.*, *121*, 1–14.

Johnson, J. B., and M. Ripepe (2011), Volcano infrasound: A review, *J. Volcanol. Geotherm. Res.*, *206*, 61–69.

Johnson, J. B., J. F. Anderson, R. E. Anthony, and M. Sciotto (2013), Detecting geyser activity with infrasound, *J. Volcanol. Geotherm. Res.*, *256*, 105–117, doi:10.1016/j.jvolgeores.2013.02.016.

Kamo, K., K. Ishihara, and M. Tahira (1994), Infrasonic and seismic detection of explosive eruptions at Sakurajima volcano, Japan, and the PEGASAS-VE early-warning system, in *Proceedings of the First International Symposium on Volcanic Ash and Aviation Safety*, pp. 357–365, U. S. Geological Survey Bulletin 2047.

Kenny, R. J., C. Hobbs, K. Plotkin, and D. Pilkey (2009), Measurement and characterization of Space Shuttle solid rocket motor plume acoustics, *AIAA Paper*, May 2009-3161, Miami, Fla.

Kieffer, S. W., and B. Sturtevant (1984), Laboratory studies of volcanic jets, *J. Geophys. Res.*, *89*(B10), 8253–8268.

Kim, K., and J. M. Lees (2011), Finite-difference time-domain modeling of transient infrasonic wave fields excited by volcanic explosions, *Geophys. Res. Lett.*, *38*, L06804, doi:10.1029/2010GL046615.

Kim, K., J. M. Lees, and M. Ruiz (2012), Acoustic multipole source model for volcanic explosions and inversion for source parameters, *Geophys. J. Int.*, *191*, 1192–1204.

Kundu, P. K., and I. M. Cohen (2008), *Fluid Mechanics,* 4th ed., Academic Press, Burlington, Mass.

Lacanna, G., and M. Ripepe (2013), Influence of near-source volcano topography on the acoustic wave field and implication for source modeling, *J. Volcanol. Geotherm. Res.*, *250*, 9–18.

Le Pichon, A., E. Blanc, and A. Hauchecorne (2010), *Infrasound Monitoring for Atmospheric Studies*, Springer, Berlin.

Leehey, P., and C. E. Hanson (1971), Aeolian tones associated with resonant vibration, *J. Sound Vib.*, *13*(4), 465–483.

Leishman, T. W., S. Rollins, and H. M. Smith (2006), An experimental evaluation of the regular polyhedron loudspeakers as omnidirectional sources of sound, *J. Acoust. Soc. Am.*, *120*(3), 1411–1422.

Lighthill, J. (1978), *Waves in Fluids,* 2nd ed., Cambridge Univ. Press, Cambridge, U. K.

Lighthill, M. J. (1952), On sound generated aerodynamically I. General theory, *Proc. R. Soc. London, Ser. A*, *211*, 564–581.

Lighthill, M. J. (1954), On sound generated aerodynamically II. Turbulence as a source of sound, *Proc. R. Soc. London, Ser. A*, *222*, 1–32.

Lighthill, M. J. (1962), The Bakerian Lecture, 1961: Sound generated aerodynamically, *Proc. R. Soc. London, Ser. A*, *267*(1329), 147–182.

Lighthill, M. J. (1963), Jet noise, *AIAA J.*, *1*(7), 1507–1517.

Lilley, G. M. (1991), Jet noise classical theory and experiments, in *Aeroacoustics of Flight Vehicles: Theory and Practice,* vol. 1, edited by H. H. Hubbard, pp. 211–289, Acoustical Society of America, Melville, N. Y.

Marchetti, E., M. Ripepe, A. J. L. Harris, and D. Delle Donne (2009), Tracing the differences between Vulcanian and Strombolian explosions using infrasonic and thermal radiation energy, *Earth Planet. Sci. Lett.*, *279*(2-3), 273–281.

Marcillo, O., and J. B. Johnson (2010), Tracking near-surface atmospheric conditions using an infrasound network, *J. Acoust. Soc. Am.*, *128*(1), EL14–EL19.

Matoza, R. S., D. Fee, M. Garces, J. M. Seinar, P. A. Ramon, and M. A. H. Hedlin (2009a), Infrasonic jet noise from volcanic eruptions, *Geophys. Res. Lett.*, *36*, L08303, doi:10.1029/2008GL036486.

Matoza, R. S., A. Le Pichon, J. Vergoz, P. Herry, J. Lalande, H. Lee, I. Che, and A. Rybin (2011), Infrasonic observations of the June 2009 Sarychev Peak eruption, Kuril islands: Implications for infrasonic monitoring of

remote explosive volcanism, *J. Volcanol. Geotherm. Res.*, *200*, 35–48, doi:10.1016/j.jvolgeores.2010.11.022.

Matoza, R. S., M. A. Garces, B. A. Chouet, L. D'Auria, M. A. H. Hedlin, C. De Groot-Hedlin, and G. P. Waite (2009b), The source of infrasound associated with long-period events at Mount St. Helens, *J. Geophys. Res.*, *114*, B04305, doi:10.1029/2008JB006128.

Morse, P. M., and K. U. Ingard (1968), *Theoretical Acoustics*, McGraw-Hill, Princeton, N. J.

Neilsen, T. B., K. L. Gee, A. T. Wall, and M. M. James (2013a), Similarity spectra analysis of high-performance jet aircraft noise, *J. Acoust. Soc. Am.*, *133*, 2116–2125.

Neilsen, T. B., K. L. Gee, A. T. Wall, M. M. James, and A. A. Atchley (2013b), Comparison of supersonic full-scale and laboratory-scale jet data and the similarity spectra for turbulent mixing noise, *Proc. Meetings Acoust.*, *19*, 040071.

Pierce, A. D. (1989), *Acoustics: An Introduction to its Physical Principals and Applications*, Acoustical Society of America, Melville, N. Y.

Ripepe, M., C. Bonadonna, A. Folch, D. Delle Donne, G. Lacanna, E. Marchetti, and A. Höskuldsson (2013), Ash-plume dynamics and eruption source parameters by infrasound and thermal imagery: The 2010 Eyjafjallajökull eruption, *Earth Planet. Sci. Lett.*, *366*, 112–121.

Ripepe, M., S. De Angelis, G. Lacanna, P. Poggi, C. Williams, E. Marchetti, D. Delle Donne, and G. Ulivieri (2009), Tracking pyroclastic flows at Soufriere Hills Volcano, *Eos Trans. AGU*, *90*(27), 229–236.

Schlinker, R. H., S. A. Liljenberg, D. R. Polak, K. A. Post, C. T. Chipman, and A. M. Stern (2007), Supersonic jet noise characteristics and propagation: Engine and model scale, *13th AIAA/CEAS Aeroacoustics Conference,* Rome, Italy, AIAA (2007-3623).

Sparks, R. S. J., M. I. Burski, S. N. Carey, J. S. Gilbert, L. S. Glaze, H. Sigurdsson, and A. W. Woods (1997), *Volcanic Plumes*, Wiley-Blackwell, New York.

Taddeucci, J., P. Scarlato, A. Capponi, E. Del Bello, C. Cimarelli, D. M. Palladino, and U. Kueppers (2012), High-speed imaging of Strombolian explosions: The ejection velocity of pyroclasts, *Geophys. Res. Lett.*, *39*, L02301, doi:10.1029/2011GL050404.

Tam, C. K. W. (1998), Jet noise: Since 1952, *Theor. Comput. Fluid Dyn.*, *10*, 393–405.

Tam, C. K. W. (2004), Computational aeroacoustics: An overview of computational challenges and applications, *Int. J. Comput. Fluid Dyn.*, *18*(6), 547–567.

Tam, C. K. W. (2006), Dimensional analysis of jet noise data, *AIAA J.*, *44*, 512–522.

Tam, C. K. W., and D. E. Burton (1984), Sound generated by instability waves of supersonic flows 2. Axisymmetric jets, *J. Fluid Mech.*, *138*, 273–295.

Tam, C. K. W., M. Golebiowski, and J. M. Seiner (1996), On the two components of turbulent mixing noise from supersonic jets, *AIAA Pap., 96-1716*, State College, Penn.

Tam, C. K. W., K. Viswanathan, K. K. Ahuja, and J. Panda (2008), The sources of jet noise: Experimental evidence, *J. Fluid Mech.*, *615*, 253–292.

Vergniolle, S., and J. Caplan-Auerbach (2006), Basaltic thermals and subplinian plumes: Constraints from acoustic measurements at Shishaldin volcano, Alaska, *Bull. Volcanol.*, *68*, 611–630.

Viswanathan, K. (2004), Aeroacoustics of hot jets, *J. Fluid Mech.*, *516*, 39–82.

Viswanathan, K. (2006), Scaling laws and a method for identifying components of jet noise, *AIAA J.*, *44*(10), 2274–2285.

Viswanathan, K. (2007), Improved method for prediction of noise from single jets, *AIAA J.*, *45*(1), 151–161.

Viswanathan, K. (2009), Mechanisms of jet noise generation: Classical theories and recent developments, *Int. J. Aeroacoust.*, *8*(4), 355–408.

Viswanathan, K., M. B. Alkislar, and M. J. Czec (2010), Characteristics of the shock noise component of jet noise, *AIAA J.*, *48*(1), 25–46.

Wang, M., J. B. Freund, and S. K. Lele (2006), Computational prediction of flow-generated sound, *Annu. Rev. Fluid Mech.*, *38*, L483–L512, doi:10.1146/annurev.fluid.38.050304.092036.

Woulff, G., and T. R. McGetchin (1976), Acoustic noise from volcanoes: Theory and experiment, *Geophys. J. R. Astron. Soc.*, *45*, 601–616.